ECCOMAS Congress 2016
VII European Congress on Computational Methods in Applied Sciences and Engineering
M. Papadrakakis, V. Papadopoulos, G. Stefanou, V. Plevris (eds.)
Crete Island, Greece, 5–10 June 2016

A MORE COMPREHENSIVE MODELING OF CONTACT FORCE DURING SHEAR TESTING USING DEM

Varvara Roubtsova[1] **and Mohamed Chekired**[1]

[1] Institut de recherche d'Hydro-Québec (IREQ),
Expertise Sciences des matériaux
Varennes, Québec, Canada
e-mail: roubtsova.varvara@ireq.ca

Keywords: Discrete Element Method (DEM), Shear Test, Energy-Work Balance, High Performance Parallel Computing (HPPC).

Abstract. *The subject of this paper is a visualization tool which may prove helpful for understanding the highly complex responses of granular systems during shear tests. The motivation of such approach is to face the challenge related to the micro scale contact forces in a granular system. The Discrete Element Method (DEM) was used to simulate shear testing on an assembly of spherical glass beads. All simulations were performed using the 3D virtual laboratory SiGran. The macro-scale response of the granular system is presented, including energy and force distributions. Two particle-size distributions were considered in the study to validate the virtual approach. The influence of the contact model is also a part of this study.*

1 INTRODUCTION

In this paper, we present a first attempt to assess the different types of energy involved in granular systems at a particle scale by using the Discrete Element Method (DEM). Continuum approaches do not take into account the particulate nature of the granular system, in which overall deformation is essentially the effect of two non-linear and irreversible processes: relative sliding between particles, and rotation of particles. Because of their particulate nature, granular systems exhibit highly complex responses to applied load. For practical purposes, then, it is important to consider this particulate nature in order to overcome the limitations of continuum approaches. Being discrete in nature, DEM [1] is able to model the motion of a particle assembly without losing or neglecting the individual characteristics of each particle. The granular system could either be saturated with water or have other fluids or/and gases in the voids. A virtual laboratory named SiGran was developed by Hydro-Quebec's research institute (IREQ) to mimic the different experimental tests that are standard for soil sciences and also to better understand the different phenomena that occur at the micro level during those tests. The visualization features of this laboratory help to access information that is very difficult or impossible to study in real experiments. The description of work conducted with SiGran can be found in the proceedings of international conferences [2-4]. SiGran is based on coupling of DEM and MAC (Marker-And-Cell [5]) methods. Additionally, we assume a dry particle assembly, excluding any kind of attraction forces. A description of the MAC method is absent here but can be found in [6].

In the present study, a validation was first performed by comparing the DEM simulation results with the experimental ones obtained by [7] at a macro-scale on a sheared granular system made up of mono-disperse idealized spherical particles. In the second phase, the model was applied to poly-disperse idealized spherical particles.

2 DISCRETE ELEMENT METHOD

The Discrete Element Method (DEM) describes the motion of particle assemblies and has been widely used as a mathematical tool studying their behavior. DEM was introduced by Cundall in 1971 [1] for the analysis of rock mechanics and was applied to soils by Cundall and Strack in 1979 [8]. It is based on Newton's second law of motion. An explicit time stepping scheme is used for integration in time. The behavior of the particle assembly under external loading at a given time step can be described using information from the previous time step, including the dimensions of each particle, its position relative to adjacent particles and the relative velocities (displacement and rotation) of neighboring particles. The contact forces acting on the particle are calculated from this data, and the acceleration, velocity and position at the new time step are determined. The concept of interactive forces between particles is illustrated in Figure 1.

The fundamental equations of motion for the i^{th} particle are as follows (the subscript j refers to the j^{th} neighboring particle, and k is the number of neighboring particles):

$$m_i \frac{d\vec{V}_i}{dt} = m_i \vec{g} + \sum_{j=1}^{k} \left(\vec{F}_{cn,ij} + \vec{F}_{dn,ij} + \vec{F}_{ct,ij} + \vec{F}_{dt,ij} \right) \tag{1}$$

$$I_i \frac{d\vec{\omega}_i}{dt} = \sum_{j=1}^{k} \left(\vec{T}_{ij} + \vec{M}_{ij} \right) \tag{2}$$

Where:

m_i, I_i, are the mass (kg) and moment of inertia (kg·m^2) of particle i respectively;

$\vec{V}_i$ and $\vec{\omega}_i$ are the translational (m/s) and rotational (s^{-1}) velocities of particle i;

$\vec{F}_{cn,ij} = -K_n \delta_n^{\frac{3}{2}} \vec{n}$ is the normal force of contact (N);

$\vec{F}_{dn,ij} = -C_n \vec{V}_{n,ij}$ and $\vec{F}_{dt,ij} = -C_t \vec{V}_{t,ij}$ are the normal and tangential damping forces (N) respectively;

$\vec{F}_{ct,ij}$ is the tangential force of contact (N); this force will be discussed in detail later;

$\vec{T}_{ij} = R_i \left(\vec{F}_{ct,ij} + \vec{F}_{dt,ij} \right)$ is the rolling torque (N·m);

$\vec{M}_{ij} = -\mu_r \left| \vec{F}_{cn,ij} \right| \frac{\vec{\omega}_i}{\left| \vec{\omega}_i \right|}$ is the friction torque (N·m);

$K_n = \frac{4}{3} E^* \sqrt{R^*}$, $C_n = D_n \sqrt{6 m^* E^* \sqrt{R^* \delta_n}}$, $C_t = D_t \sqrt{6 m^* E^* \sqrt{R^* \delta_n}}$

δ_n, δ_t are the normal and tangential contact displacement respectively;

$\frac{1}{E^*} = \frac{1-\nu_i^2}{E_i} + \frac{1-\nu_j^2}{E_j}$ and $\frac{1}{R^*} = \frac{1}{|R_i|} + \frac{1}{|R_j|}$

Where E is Young's modulus (Pa), ν is the Poisson ratio, R_i is the particle radius (m), μ_r is the rolling (m) friction coefficient, and D_n and D_t are the normal and tangential damping coefficients respectively.

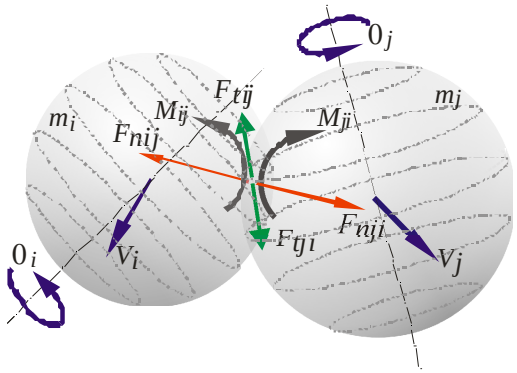

Figure 1. Interactive forces between two particles

3 TANGENTIAL FORCE MODELS

A wide range of tangential forces models are available for DEM [9]. The theoretical basis for a complex approach was proposed by Mindlin and Deresiewicz [10] for elastic materials based on Hertz theory. According this theory, the actual tangential force depends on the whole loading history and also on the instantaneous rate of change of the normal force or displacement. The tangential force is given by:

$$\frac{dF_{ct,ij}}{dt} = K_t \nu_t \qquad (3)$$

Where: $K_t = 2\sqrt{R^* \delta_n} \left(\frac{G_i}{2-\nu_i} + \frac{G_j}{2-\nu_j} \right)$

G is the shear modulus; v_t is a relative tangential velocity between surfaces in contact.
A complete loading force-displacement path can be built through successive incremental steps. A limit on the maximum tangential stress exists as stated by Coulomb's law of friction and is expressed as follows:

$$\left|F_{ct,ij}\right| \leq \mu_s F_{cn,ij} \quad (4)$$

Where μ_s is the sliding friction coefficient.

More details and analysis of loading and unloading curves for specific cases can be found in [11] and [12].

The SiGran programming code uses a high level of data parallelism on NVIDIA Graphics Processing Units (GPU) based on Tesla High Performance Computing (HPC) hardware. The forces acting on each inter-particle contact at each step of time are computed on its own GPU-kernel. Thousands of contacts are thus processed at the same time. In addition, one contact usually lasts several time steps, and several contacts can begin or end during a given time step. In theory, each particle can have more than one contact with all of the particles in the assembly during an experiment. For calculation purposes, only the history for the acting contact must be stored. This history begins with the first contact of specific particles, and it can be ended after loss of contact. A special algorithm, optimized for GPU calculations, was introduced into SiGran to maintain the history of each contact. This algorithm takes into account the maximum possible contacting particles, which depends on the relative particle size (i.e., the biggest and the smallest) in the assembly and a memory model of the GPU to minimize calculation time.

The simplest tangential forces model uses only the maximum force obtained by Coulomb's law. In this case, no history of contact is considered, which simplifies the algorithm and significantly reduces calculation time and used memory. In the case of SiGran, this is overall shared GPU memory.

4 DIRECT SHEAR TEST

The direct shear test is one of the oldest soil strength tests performed in the laboratory. Even though it has some disadvantages, as documented in ASTM D 3080 – 98 [13], it is routinely used by geotechnical engineers to determine the shear strength parameters of soil essential for stability assessment. The first direct shear apparatus was built by Alexander Collin in 1846 to measure the strength of a clay soil shear for purposes of slope stability assessment [14, 13]. The current version of the direct shear apparatus was designed by Casagrande in 1932. Figure 2 shows a schematic representation of the shear box.

A normal load is applied to the specimen before shearing across the predetermined horizontal plane between the two halves of the shear box. Measurements of shear load, shear displacement and normal displacement are recorded. From these results, the shear strength parameters can be determined.

4.1 Physical direct shear test on spherical mono-disperse chrome steel particles

The shear tests performed on spherical chrome steel particles are described in [7]. A square metal box, cross-section 60 x 60 mm, was filled with 11,700 chrome steel particles with a sphere radius of 0.992mm. The material density was 7,800 kg/m^3, the shear modulus was 7.9 x 10^{10}Pa, and the Poisson's ratio was 0.28. The average friction coefficient of 0.096 was measured in [16], and the sphere-boundary friction coefficient for the shear box was 0.175. The force required to maintain the fixed section of the box in a stationary position was measured using a load cell. The normal stress was 55 kPa.

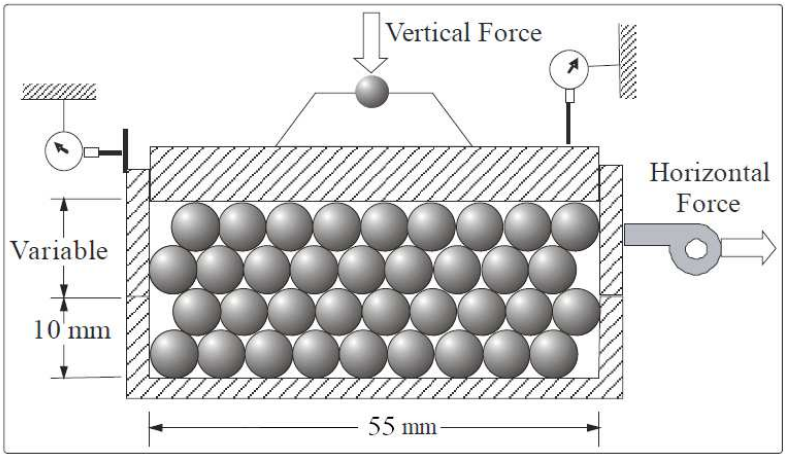

Figure 2: Schematic representation of a shear box

4.2 Numerical simulation of direct shear test with spherical mono-disperse chrome steel particles

The shear test simulation was conducted with SiGran. The forces applied on each box wall were calculated by summing the contact forces during interaction between particles and boundaries. The comparison between the experimental data and numerical results is shown in Figure 3. The shear stress was determined as in the experiment: the total of particle forces applied on the fixed section of the box was divided by the original cross-section area. The overall shear strain, as proposed in [7], is considered to be the displacement of the moving section of the box divided by the initial height of the sample. The vertical strain is taken to be the ratio of the vertical displacement of the upper half of the shear box to the original height of the samples. The difference in vertical stress results between the laboratory tests and the DEM simulations is most likely due to initial preloading and better arrangement for the simulation. The increase in the inter-particle friction coefficient during a shear test also contributed to the difference in the results.

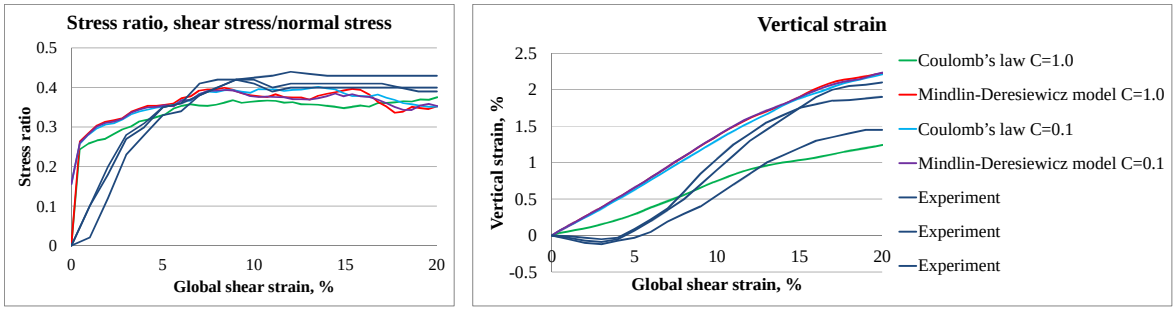

(a) (b)

Figure 3. Comparison of numerical and experimental data

The numerical simulations for two tangential force models were conducted with two values of Courant's number that differed by a factor of 10 (1.0 and 0.1). Courant's number is known for its connection with the Courant-Friedrichs-Lewy convergence condition for solving partial differential equations. The time step is calculated using the following formula:

$$\Delta t \leq C \min \sqrt{\frac{m}{K_n}} \tag{4}$$

Where:
C is a Courant number
m is the mass of the particle
K_n is a normal stiffness coefficient (see Formula 1)

The results for the Mindlin-Deresiewicz model are independent of the number of iterations during a particle contact, in contrast with Coulomb's low, which is dependent on that value.

As mentioned before, numerical simulation gives access to more parameters than physical experiments. The real tangential force can be obtained from the force equilibrium on the shear box in the shear direction. All forces acting on the boundaries in the shear direction are shown in figure 4.

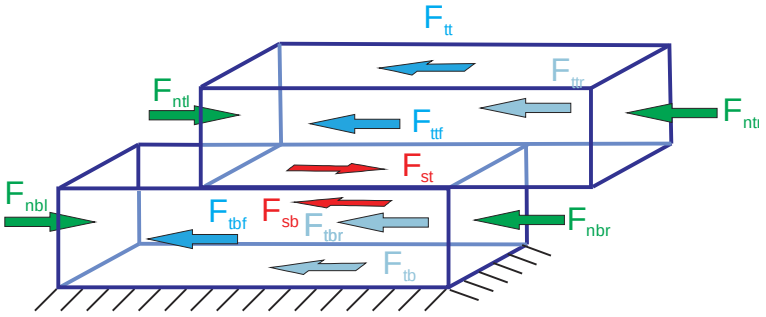

Figure 4. Forces acting in shear direction

The following expressions can be written to find the shear forces involved in the upper and lower halves of the shear box:

$$\begin{aligned} F_{st} &= F_{ntl} - F_{ntr} - F_{tt} - F_{ttf} - F_{ttr} \\ F_{sb} &= F_{nbr} - F_{nbl} + F_{tb} + F_{tbf} + F_{tbr} \end{aligned} \quad but\ F_{st} = F_{sb} \tag{5}$$

Where:
F_{st} : Shear force obtained from the equilibrium of the upper half of the shear box (N)
F_{sb} : Shear force obtained from the equilibrium of the lower half of the shear box (N)
F_{ntl} : Normal force on the left boundary of the upper half of the shear box (N)
F_{nbl} : Normal force on the left boundary of the lower half of the shear box (N)
F_{ntr} : Normal force on the right boundary of the upper half of the shear box (N)
F_{nbr} : Normal force on the right boundary of the lower half of the shear box (N)
F_{tt} : Tangential (friction) force on the top surface of the upper half of the shear box (N)
F_{tb} : Tangential (friction) force on the down surface of the lower half of the shear box (N)
F_{ttf} : Tangential (friction) force on the front surface of the upper half of the shear box (N)
F_{tbf} : Tangential (friction) force on the front surface of the lower half of the shear box (N)
F_{ttr} : Tangential (friction) force on the rear surface of the upper half of the shear box (N)
F_{tbr} : Tangential (friction) force on the rear surface of the lower half of the shear box (N)

Figure 5 shows the evolution of all forces on the upper and lower part of the shear box separately. These forces are obtained by simulations.

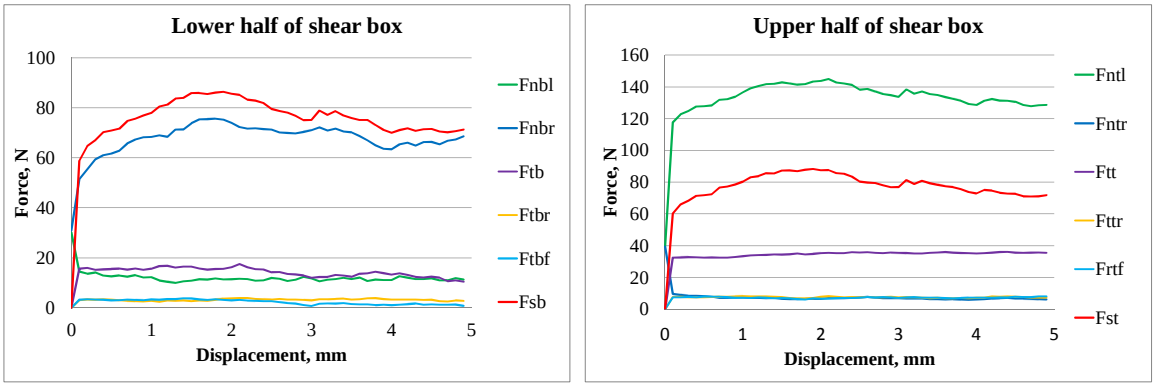

(a) (b)

Figure 5. Evolution of forces acting during the shear test

Figure 6 shows the comparison between the shear forces calculated from Formula 5 and the normal forces. The shear force can be measured during physical experiments. The shear force values calculated at the upper and lower halves are almost identical, which demonstrates a good equilibrium of forces during all simulations. This figure shows that the force needed to move the upper half of the shear box is different from the force needed to keep the lower half stationary. This difference is a result of friction between the particles and the box.

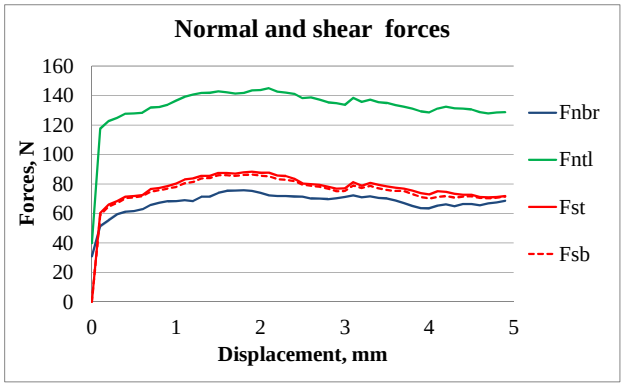

Figure 6. Normal and shear forces obtained during the shear test

4.3 Work-energy balance during shear test

The force required to move the upper section of the box accomplished work. The work done was calculated by integrating the force vector along the path traveled by the force. The total work done by all forces must be equal to the energy variation. The following types of energy were used:

- Kinetic energy, which has two parts: translation (E_{kt}) and rotation (E_{kr}):

$$E_k = E_{kt} + E_{kr} = \sum_{i=1}^{n} \frac{m_i v_i^2}{2} + \sum_{i=1}^{n} \frac{I_i w_i^2}{2}$$

Where n is the number of particles in the shear box.

- Potential energy:

$$E_p = \sum_{i=1}^{n} m_i h_i g$$

Where h_i is the distance from the bottom of the box to the particle center.

- Internal elastic energy:

$$E_s = 0.5 \cdot \sum_{i=1}^{n} \sum_{j=1}^{k} \int_0^{\delta} F_{cn} \Delta\delta = 0.5 \cdot \sum_{i=1}^{n} \sum_{j=1}^{k} \int_0^{\delta} K_n \delta^{\frac{3}{2}} \Delta\delta = \sum_{i=1}^{n} \sum_{j=1}^{k} \frac{1}{5} K_n \delta^{\frac{5}{2}}$$

Where k is a number of contacts for particle i.

- Normal dissipative energy:

$$E_{dn} = \sum_{i=1}^{n} \sum_{j=1}^{k} \int_0^{\delta} F_{dn} \Delta\delta$$

- Friction energy:

$$E_f = \sum_{i=1}^{n} \sum_{j=1}^{k} \int_0^{L} F_{ct} \Delta l$$

Where l is a tangential overlap during of contact (m).

- Tangential dissipative energy

$$E_{dt} = \sum_{i=1}^{n} \sum_{j=1}^{k} \int_0^{L} F_{dt} \Delta l$$

- Rotation energy:

$$E_M = \sum_{i=1}^{n} \sum_{j=1}^{k} \int_0^{\varphi} T_i \Delta\varphi = \sum_{i=1}^{n} \sum_{j=1}^{k} \int_0^{\varphi} r_i \left(\overline{F}_{ct} + \overline{F}_{dt}\right) \Delta\varphi$$

Where φ is a rotational angle of particle i (rad).

Note that this type of energy can be included in tangential energy by including rotation in the tangential overlap.

- Dissipative rotational energy:

$$E_{dM} = \sum_{i=1}^{n} \sum_{j=1}^{k} \int_0^{\varphi} M_i \Delta\varphi$$

More details about the calculation of energy using SiGran can be found in [17].

Figure 7 shows the work-energy balance and also the contribution of the normal forces applied to move the half box and accomplish the total work.

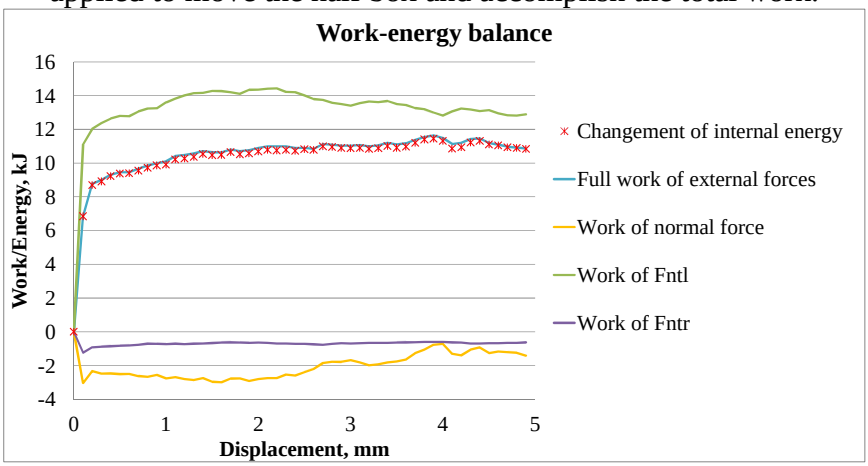

Figure 7. Work-Energy balance during the shear test

Figure 8 shows the contribution of each type of energy in the total energy balance of the system. It is clear that the main work of external forces is expended by the dissipation of energy during inter-particle and particle-wall friction. The others type of energies are shown

in Figure 8 b and 8c in which the scale of the vertical axe has been changed. Figure 9 shows the distribution of different energies among the particles. The dissipative types of energy were calculated cumulatively from the beginning of the shear experiment without considering the energy scattered during sample formation. Inter-particle force distribution during shear testing is shown in Figure 10.

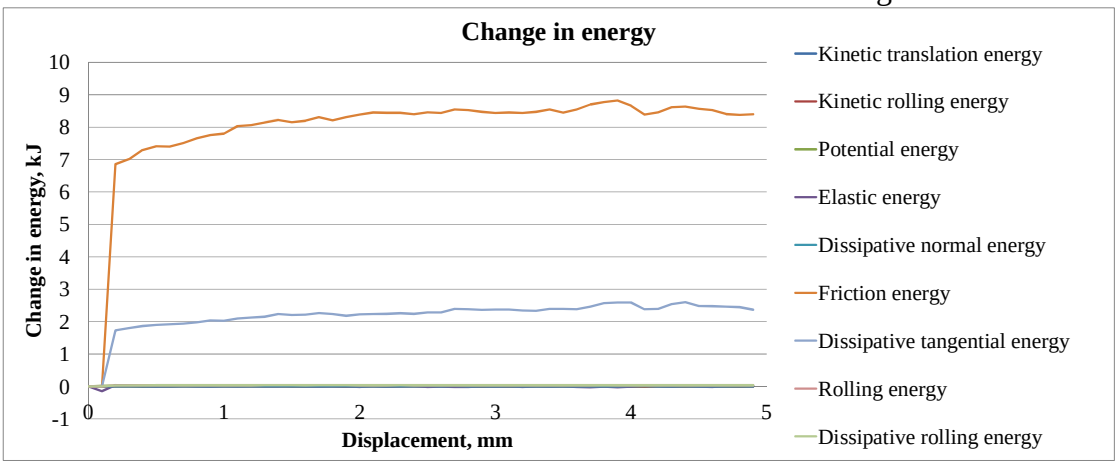

(a)

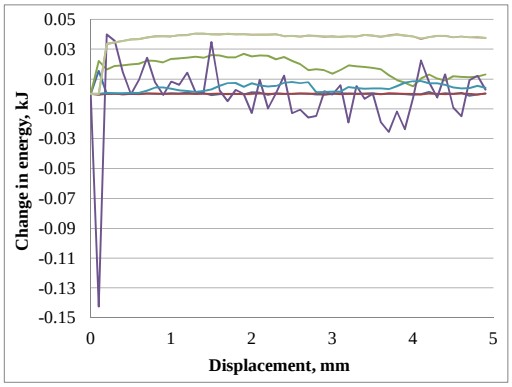

(b)

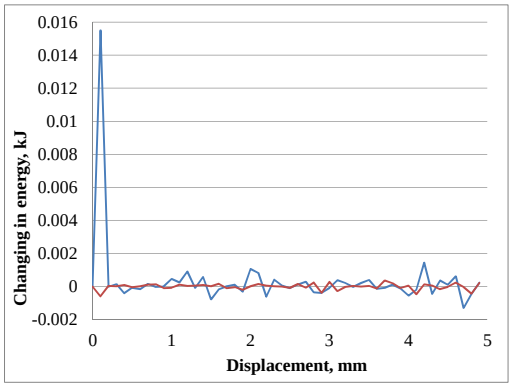

(c)

Figure 8. Change in energy during shear testing

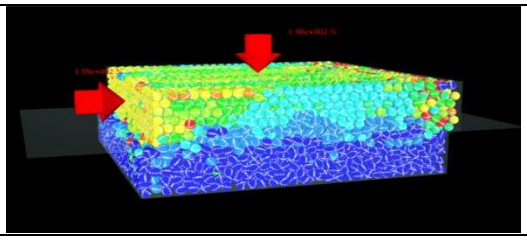

(a) Kinetic translation energy

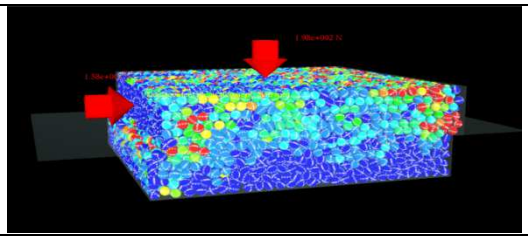

(b) Kinetic rotation energy

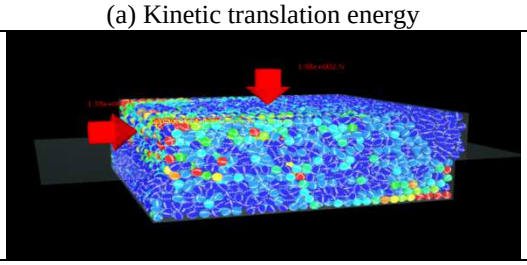

(c) Elastic energy

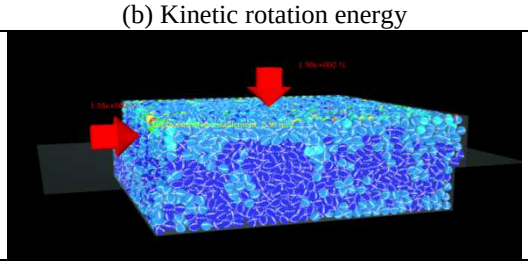

(d) Dissipative normal direction energy

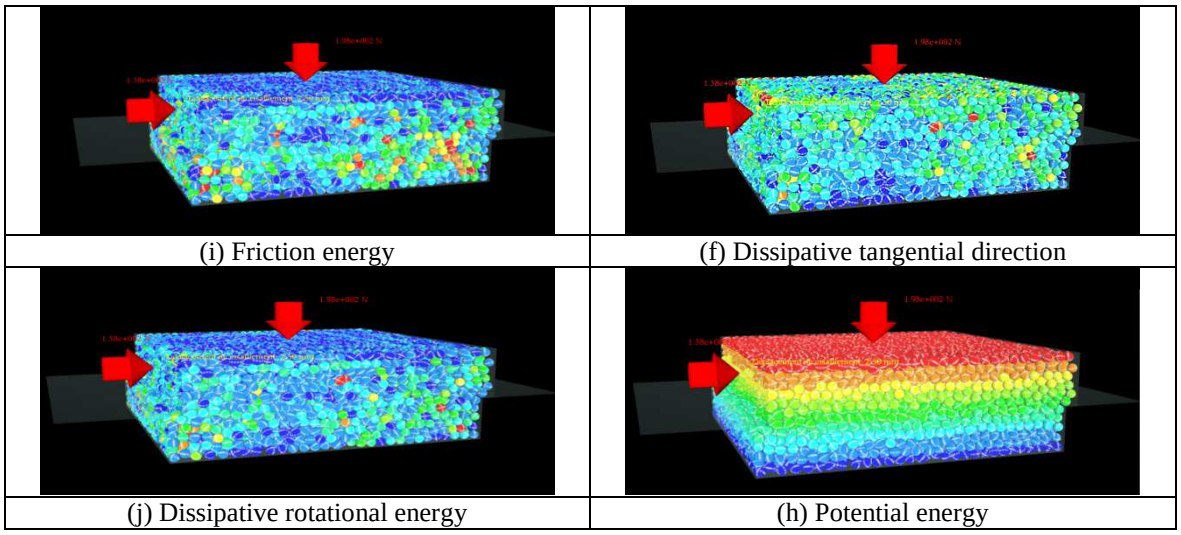

(i) Friction energy | (f) Dissipative tangential direction

(j) Dissipative rotational energy | (h) Potential energy

Figure 9. Distribution of different energies among particles (shear displacement = 2.5 mm)

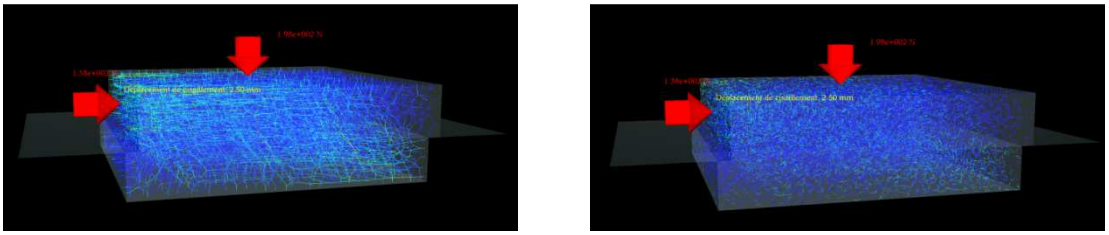

(a) Normal forces (b) Tangential forces

Figure 10. Inter-particle force distribution (shear displacement = 2.5 mm)

4.4 Simulation of shear test on poly-disperse particle assembly

The next simulation was carried out on a particle assembly having the particle size distribution presented in Figure 11. The details about this test and its comparison with experimental data can be found in [17]. Only the influence of the friction coefficient will be considered in this case. The shear tests were carried out in a box with internal dimensions of 55 x 55 mm. The samples were spherical glass beads.

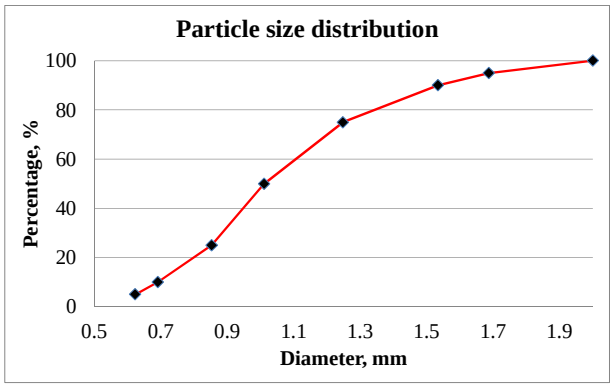

Figure 11. Particle size distribution of idealized granular media used in numerical and laboratory simulations

Young's Modulus was 68.9 GPa, Poisson's coefficient was 0.21 and the particle density was 2430 kg/m^3. To minimize the influence of wall friction, which can change the results as shown in the previous example, the friction coefficient between the walls of the shear box and

the particles was disregarded. This simplification allows us a better understanding of the inter-particle friction effect. Figure 12 shows the influence of the inter-particle friction coefficient on shear stress and vertical displacement.

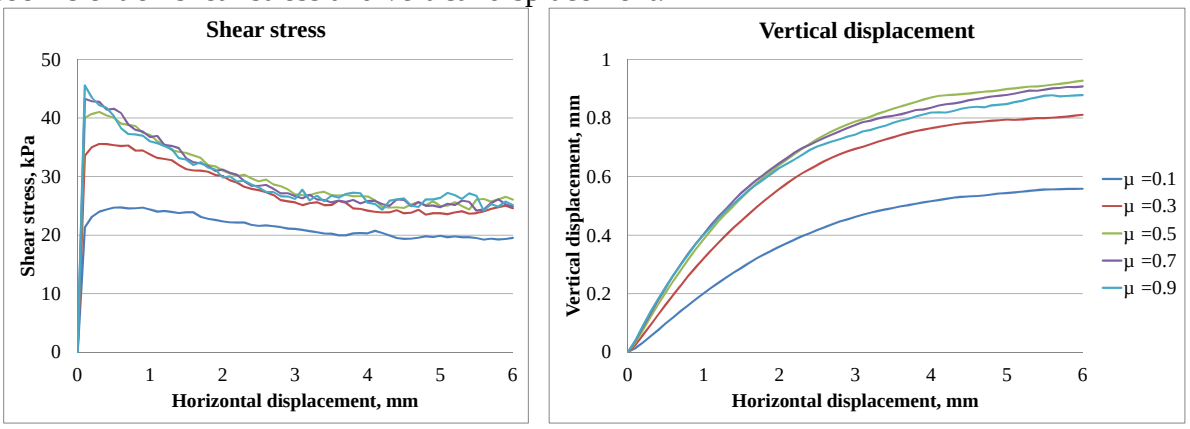

(a) (b)

Figure 12. Shear stress and vertical displacement with different friction coefficients

The influence of friction is more important at low coefficient values because the particles can slide more easily on each other. Rolling friction predominates for the highest coefficients of friction. This phenomenon can be studied by analysis of the different energy types as shown in Figure 13.

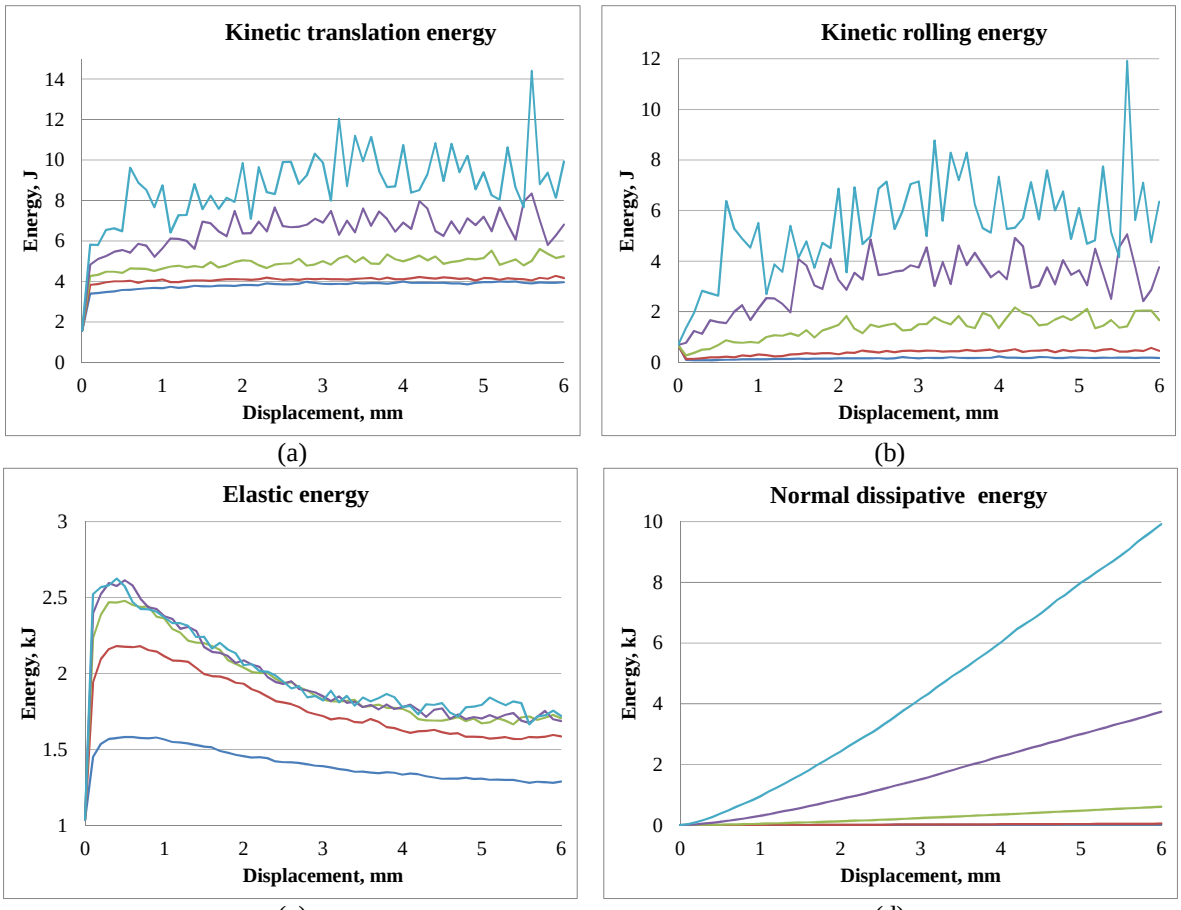

(a) (b)

(c) (d)

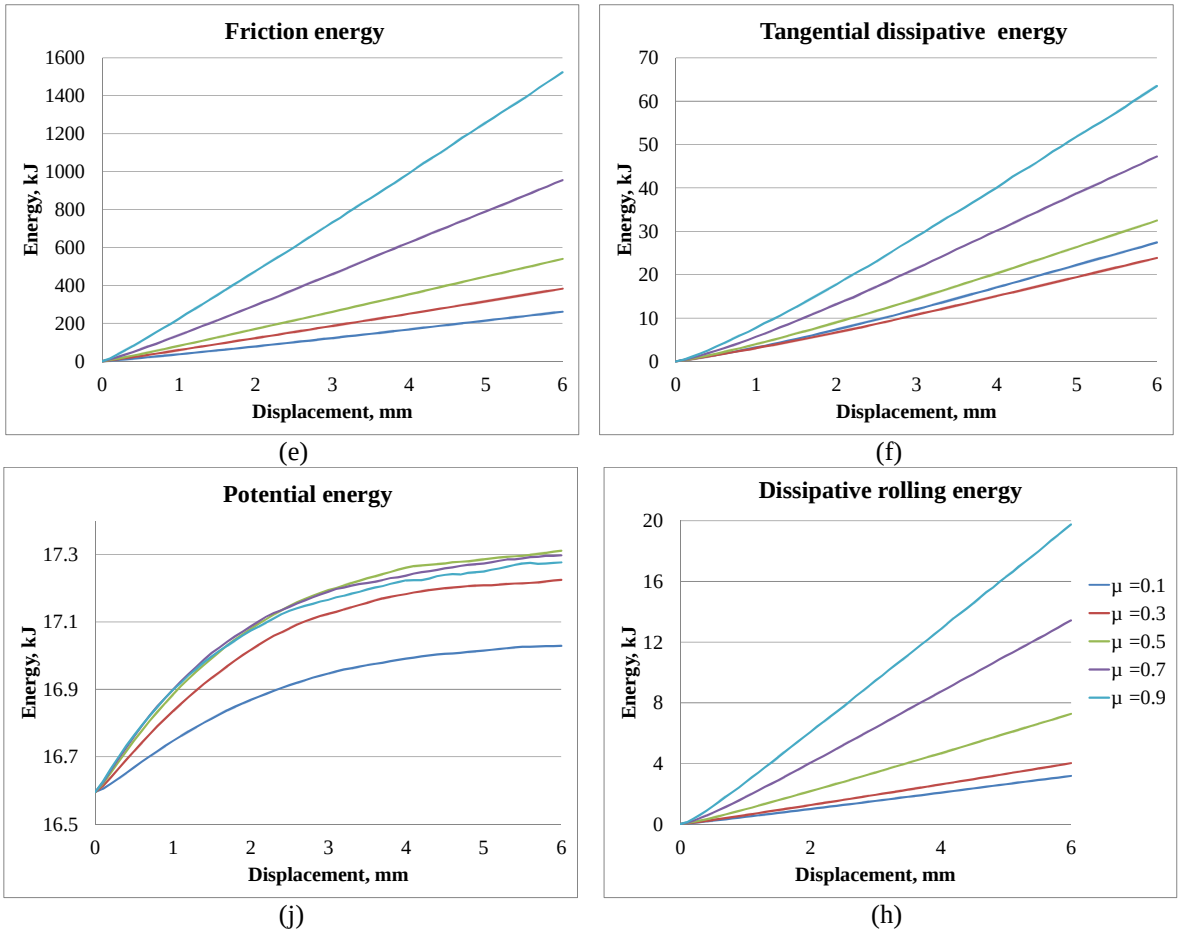

Figure 13. Variation in energies during a shear test

Figure 13 shows that the energy during the shear process increases with the friction coefficient. Due to the difficulty of sliding (see Figure 14a, b), more particles are drawn into movement, which in turn causes the dissipative energy to increase in two directions (see Figure 13d, f). The rolling motion prevails under sliding for high friction coefficients (see Figure 13b); therefore more rolling energy dissipates (see Figure 13h). The value of tangential force also increases with the friction coefficient, and thus more energy dissipates because of friction (see Figure 13e). The change in elastic energy follows the shear stress curve because the normal interaction force between the particles is the main force in this experiment. Some of the external work was spent during the movement by the interlocking of the particles on each other. There is little variation in potential energy because the vertical particle displacement is very small. The curve of potential energy follows of the change in vertical position of the top surface (see figures 12b and 13j)

Figure 14 shows the distribution of energy among particles for the maximum and minimum friction coefficients (0.1and 0.9, respectively). The area where the shear is greatest is clearly visible, and is characterized by larger relative displacements. The dissipation of energy is at its maximum at this surface. The distribution of maximum deformation of particles (elastic energy) is along the line between the upper left surface and lower right surface (Fig. 14c).

μ =0.1	μ =0.9
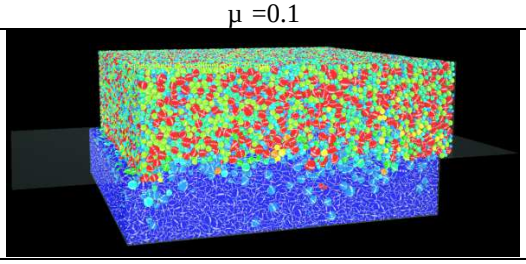	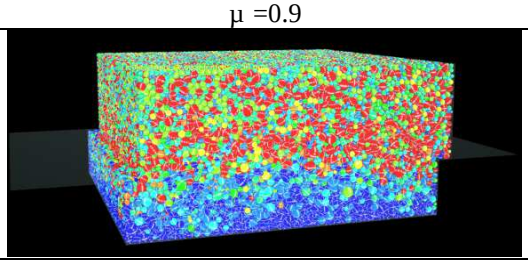
(a) Kinetic translation energy	
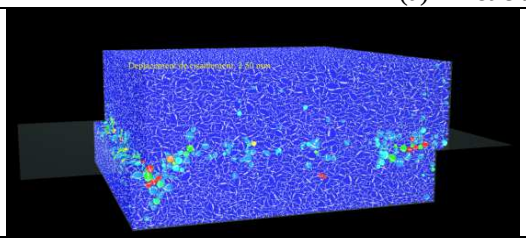	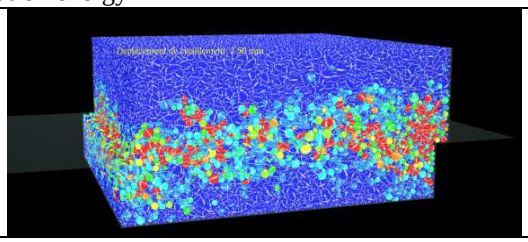
(b) Kinetic rotation energy	
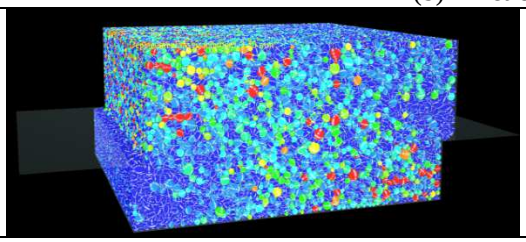	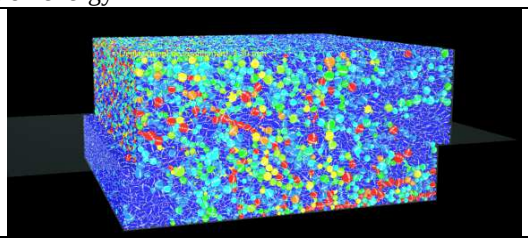
(c) Elastic energy	
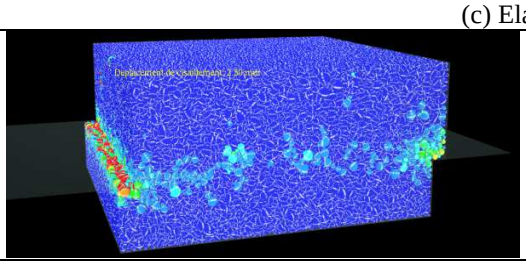	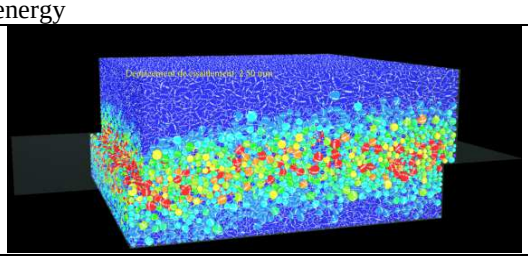
(d) Energy dissipation in normal direction	
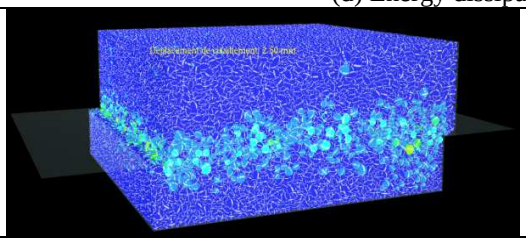	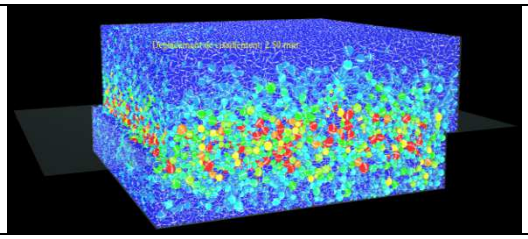
(e) Friction energy	
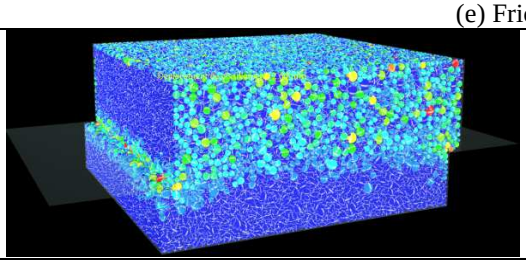	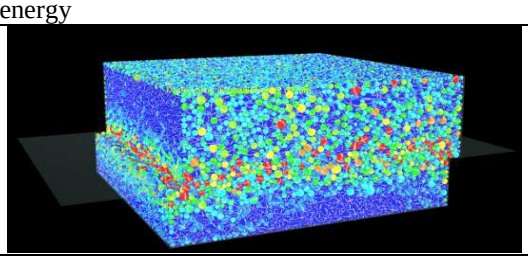
(f) Energy dissipation in tangential direction	

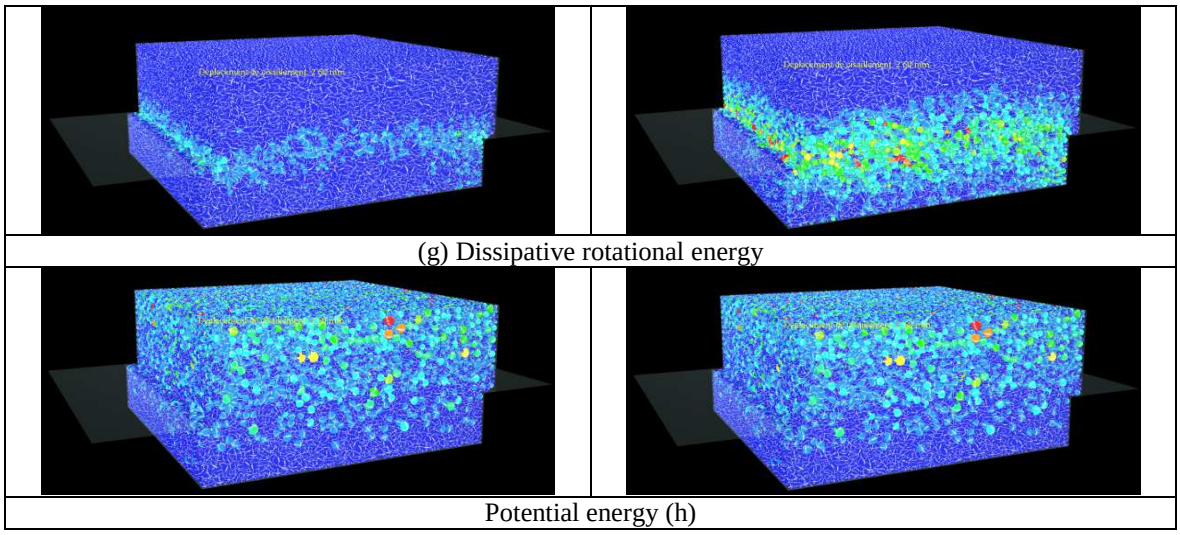

(g) Dissipative rotational energy

Potential energy (h)

Figure 14. Energy for maximum and minimum friction coefficents (displacement of 2.5 mm)

The work of external forces during the shear test is shown in Figure 15.

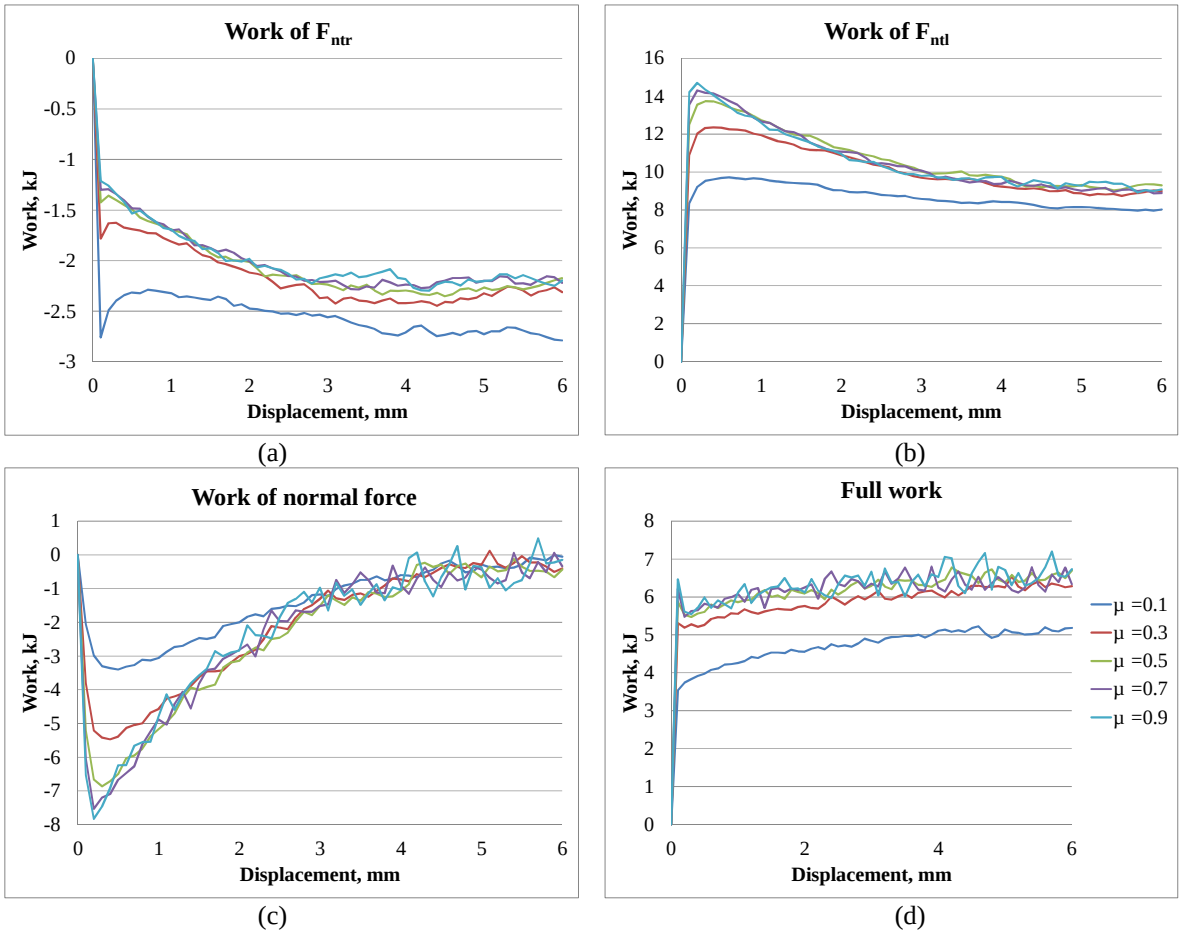

Figure 15. Work of external forces during shear test

Figure 16 shows the inter-particle force distribution before and during the shear test for the minimum and maximum friction coefficients.

5 DISCUSSION

We present a model that provides complete microscopic contact and force vector information from a 3D granular system made up of spherical particles subjected to a shear test and, consequently, all the energies can be evaluated. The obtained microscopic data allows us to quantitatively assess the relationship between the macroscopic mechanical response of the granular system and the microscopic measures such as the forces at the contact of each particle. This virtual approach has great potential for improving understanding of other granular systems, including granular response to flow, effects of particle shape and so on. This paper also presents the capability of the model to show, at each time step, images in 3D configurations. From these images, we can see the geometric properties of the particles, their contacts and also all the energy distributions in the granular assembly. Furthermore, 3D tracking of each particle can be extracted.

6 CONCLUSION

SiGran, a 3D model developed for quantitatively assessing energies involved in a granular system at a particulate scale, is presented in the current work. This model has demonstrated the ability to evaluate the change in different energies during a shear test. This powerful tool offers a new opportunity to link the energy applied to a granular system to the energies at the micro-scale.

A shear test was simulated, and the obtained results clearly indicate that the proposed model is able to solve significant problems associated with the granular system. In fact, it gives access to parameters that are impossible to reach in physical experiments. All the phenomena involved in a granular system can be captured, and the quantification of the different energies at the micro-scale can be assessed. Several findings can be used for different granular fields.

The simulation results at the macro-scale agreed well with those of physical tests. However, further work must be done to reduce the differences between simulation results and physical ones.

Extension of the current approach to soils liquefaction phenomena is underway.

μ =0.1	μ =0.9
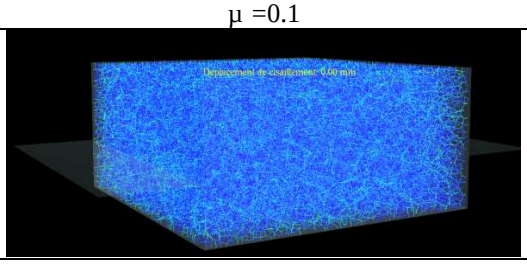	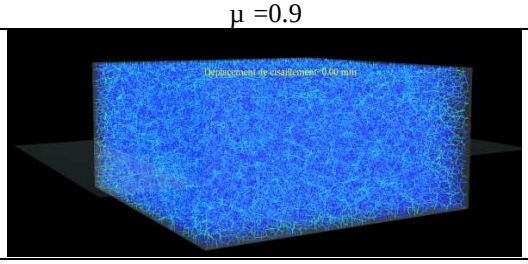
(a) Normal forces before the test (shear displacement = 0 mm)	
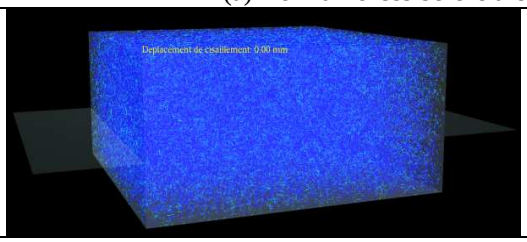	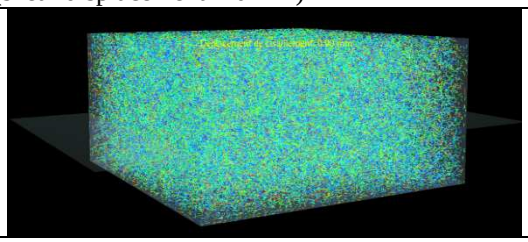
(b) Tangential forces (shear displacement = 0 mm)	

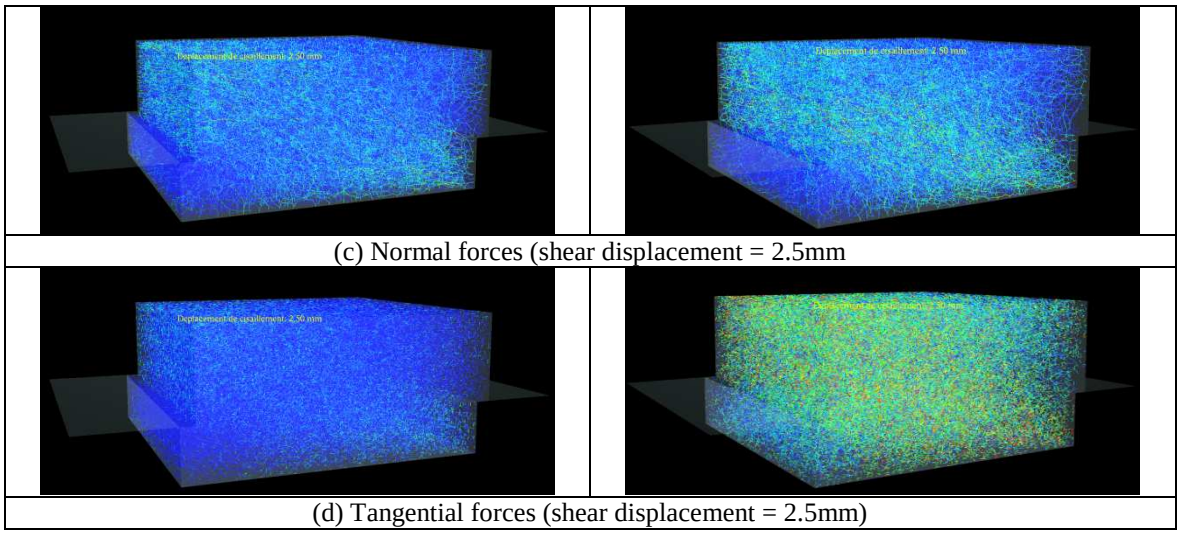

(c) Normal forces (shear displacement = 2.5mm

(d) Tangential forces (shear displacement = 2.5mm)

Figure 16. Forces during the shear test at different displacements

7 REFERENCES

[1] P. Cundall, "A computer model for simulating progressive large scale movements in blocky rock systems". *Proc. Symp. Int. Soc. Rock Mechanics*, Nancy, France, vol. 1, paper, No. II-8. (1971)

[2] V. Roubtsova, M. Chekired, B. Morin and M. Karray. "3D virtual laboratory for geotechnical applications: another perspective". Particles 2011, II International Conference on Particle-Based Methods. Fundamentals and Applications, Barcelona, Spain (2011).

[3] M. Chekired and V. Roubtsova "Virtual Reality 3D Interaction of Fluid-Particle Simulations". *V International Conference on Coupled Problems in Science and Engineering*, Ibiza, Spain, June 17-19 (2013).

[4] M. Chekired and V. Roubtsova "Pore-scale study of permeability and tortuosity for flow through particulate media using virtual approach". *ICSE-7, 7th International Conference on Scour and Erosion*, Perth, Australia, December 2–4, 2014.

[5] H. Harlow and J. E. Welch. "Numerical calculation of time-dependent viscous incompressible flow of fluid with a free surface", *The Physics of Fluids*, vol. 8, pp. 2182–2189 (1965).

[6] V. Roubtsova, M. Chekired, Y. Ethier and F. Avendano "SIMSOLS: A 3D virtual laboratory for geotechnical applications", *ICSE-6, 6th International Conference on Scour and Erosion*, Paris, France, August 27–31, (2012)

[7] L. Cui and C. O'Sullivan. 2006. "Exploring the macro- and micro-scale response of an idealized granular material in the shear apparatus", *Géotechnique*, Vol. 56, No. 7, pp. 455–468. 2006

[8] P. Cundall and O. Strack. "A discrete numerical model for granular assemblies", *Geotechnique*, Vol. 29(1), pp. 47–65. (1979).

[9] H. Kruggel-Emden, S. Wirtz and V. Scherer. . "A study on tangential force laws applicable to the discrete element method (DEM) for materials with viscoelastic or plastic behavior", *Chemical Engineering Science*, Vol. 63, Issue 6, pp. 1523–1541

(2008)

[10] R.D. Mindlin and H. Deresiewicz. “Elastic spheres in contact under varying oblique forces” *Transactions of ASME,* Series E., *Journal of Applied Mechanics*, Vol. 20, pp. 327–344. (1953)

[11] Loc Vu-Quoc and Xiang Zhang “An accurate and efficient tangential force-displacement model for elastic frictional contact in particle-flow simulations”, *Mechanics of Materials*, Vol. 31, (1999) pp. 235–269.

[12] Alberto Di Renzo and Francesco Paolo Di Maio “Comparison of contact-force models for the simulation of collisions in DEM-based granular flow codes”, *Chemical Engineering Science*, Vol. 59, pp. 525 – 541(2004)

[13] ASTM D3080 -98 ASTM D3080: Standard test method for direct shear test of soils under consolidated drained conditions (2004).

[14] Collin, “Recherches expérimentales sur les glissements spontanés des terrains argileux” Carilian-Goeurley et Delmont, Paris (1846).

[15] W. Skempton, “A slip in the west bank of the Eau Brink Cut". *Jour. Inst. Civil Engrs.*, Vol. 24, pp. 267-287 (1945).

[16] C. O’Sullivan, J.D. Bray and M.F. Riemer. “An examination of the response of regularly packed specimens of spherical particles using physical tests and discrete element simulations”, ASCE, *J. Engng Mech*., Vol. 130, No. 10, pp. 1140-1150, 2004.

[17] V. Roubtsova, M. Chekired, M. Karray and S. Amirpour. “Work-energy balance for discrete element method using shear stress tests”, *Congress on Numerical Methods in Engineering*, Lisbon, Portugal, 29 June-2 July, 2015.